The Chemistry-Forecast System at the Meteorological Service of Canada

Richard Ménard and Alain Robichaud

Meteorological Service of Canada
Dorval, Qc, CANADA

Abstract

This paper presents a real-time chemical assimilation forecast system that has been used since July 2003 as an experimental operational product at MSC (Meteorological Service of Canada).

1. Introduction

In 2001, the MSC officially implemented an operational tropospheric chemical forecast over all of North America. The system was based on an offline CTM called CHRONOS (Canadian Hemispheric and Regional Ozone and NOx system), which is driven by meteorological analyses and emissions derived from inventories. About the same time, and in collaboration with the US Environmental Protection Agency (EPA), observations collected by numerous air quality networks over many parts of Canada and the USA were made available in real time and distributed through a single web site. In the last few years, the MSC also developed an objective analysis and assimilation scheme for ozone using these observations. Since 2003, surface ozone analyses were thus produced and distributed in near real time through a web page. We will report on this chemical assimilation system, and discuss some of the findings. To conclude, we will describe our new initiative that consists of an online chemistry model coupled with the operational meteorological model GEM developed at MSC. This system can run either globally or on a limited area, and has 3D and 4D-Var capability.

2. Surface observation network

Observations of surface ozone, PM2.5 and PM10 over Canada and the USA are collected by and available from the US EPA AIRNow Data Management Center. Table 1 shows the main characteristics of these networks.

Table 1. AirNow observation network

Measurement	Units	Number of sites	Frequency	Coverage
ozone	ppmv	~ 1470	Hourly	good
PM2.5	$\mu g/m^3$	~ 550	Hourly	moderate-good
PM10	$\mu g/m^3$	~ 80	Hourly	limited

The observations are automatically screened for gross error check each hour by the US EPA, and are available 20-30 minutes past each hour. Figures 1 and 2 below show the current spatial distribution of ozone and PM2.5 observations. We note large gaps in unpopulated areas as these networks were designed originally for monitoring health effects on humans. This is however changing to get a global picture and assessment on the ecosystems, and for its use in prediction and assimilation.

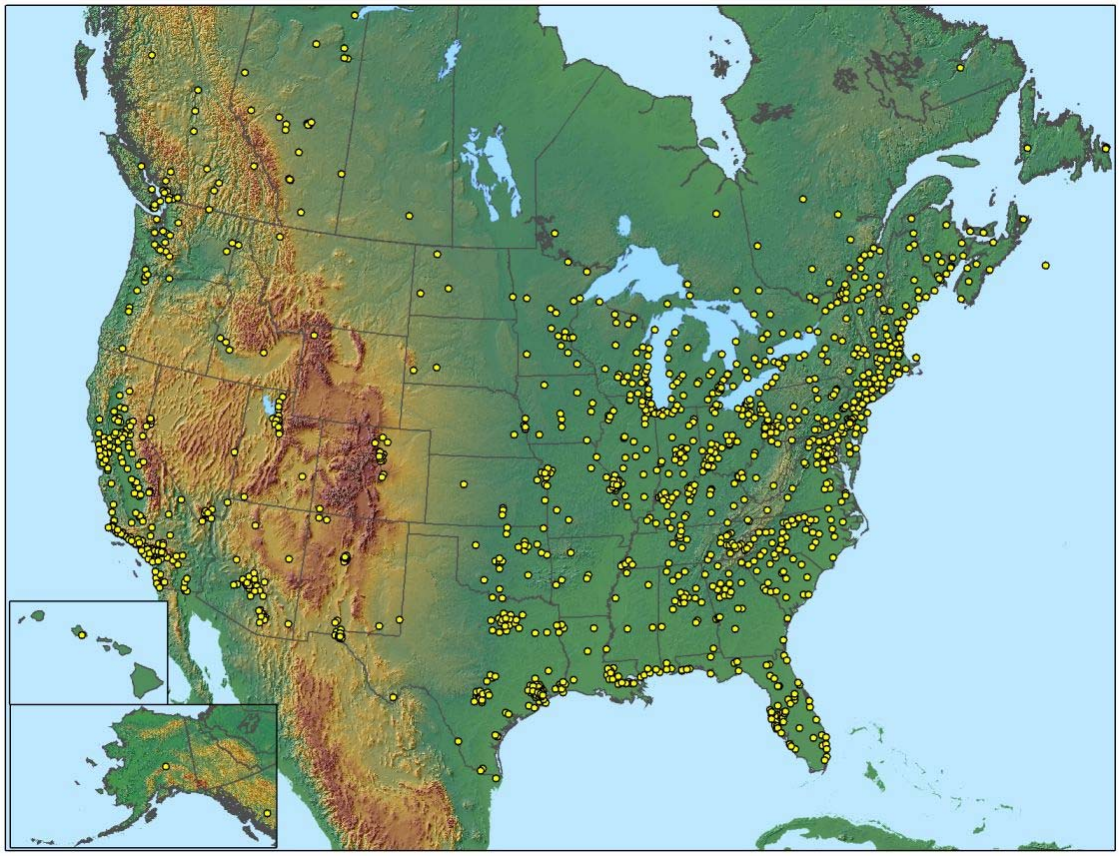

Figure 1 Surface ozone observation sites in the US EPA AIRNow (courtesy of Chet Wayland, US EPA)

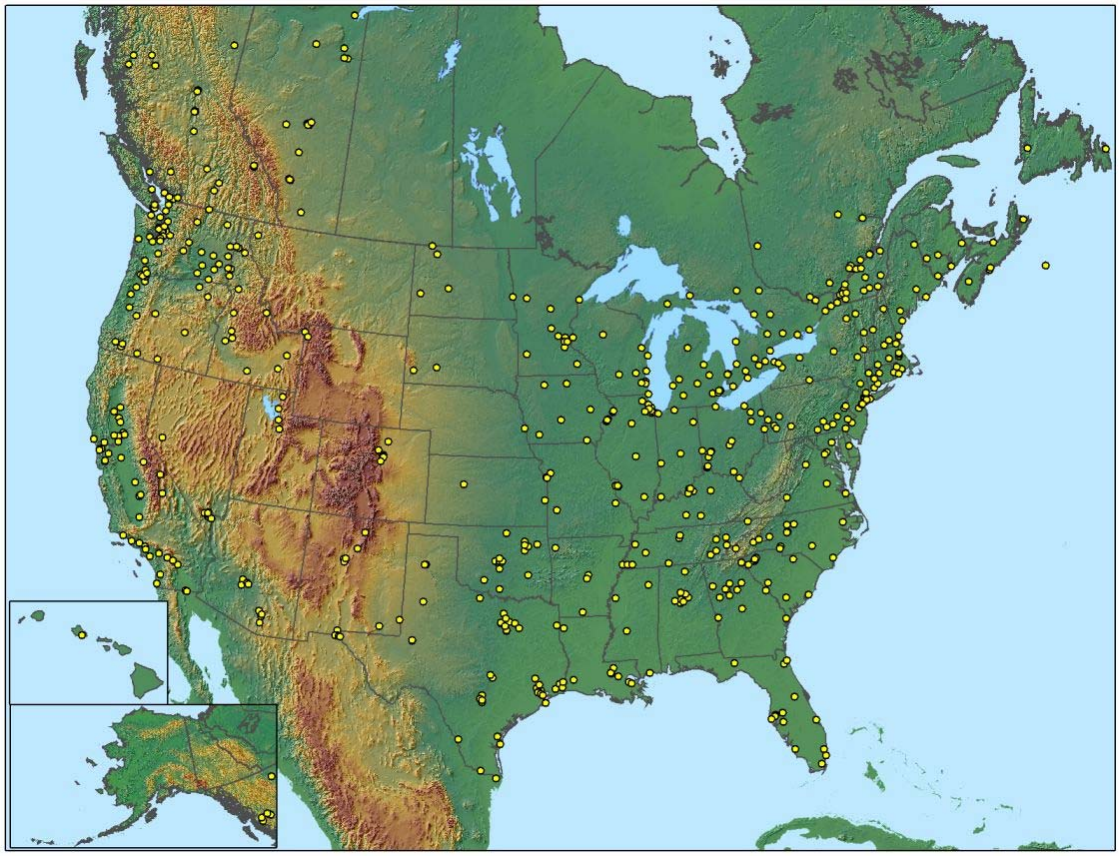

Figure 2 PM2.5 observation sites reporting to the US EPA AIRNow (courtesy of Chet Wayland, US EPA)

The US EPA is planning to upgrade his AIRNow database to have continuous measurements of precursor gases and speciation of aerosols at a limited number of sites.

The Meteorological Service of Canada has also developed a directory of monitoring networks across the US and Canada for air quality, climate and toxics measurements (not in real time). The collection of networks can be accessed from the NATChem web site www.msc-smc.ec.gc.ca/natchem/index_e.html .

3. Chemical transport model

The Canadian Hemispheric and Regional Ozone and NOx System (CHRONOS) is the CTM used in the operational air quality prediction and data assimilation. The model developed by Pudykiewicz et al. (1997) uses a terrain-following height coordinate (Gal Chen and Sommerville, 1975) from the surface to 6 km. The horizontal resolution is currently 21 km on a polar stereographic grid that covers the area depicted on the figures below. The ADOM-II chemistry due to Lurmann et al. (1986) is used with 39 gas phase advected species, and for aerosols, a 2-bin representation is used along with sedimentation. Emissions are generated by the SMOKE emission processor.

CHRONOS is run operationally once a day at 00Z for a 48 h. forecast period. The forecast of ozone, PM2.5 and PM 10 are available at http://www.msc-smc.ec.gc.ca/aq_smog/aq_guidance_e.cfm . An experimental version of the model was also run for ICARTT were 2 runs a day were made, and an assimilation of surface ozone was also carried out. The model is also run for real-time emissions scenarios were different regions have their emissions turned off. Figure 3 below shows the surface ozone when only Canadian emissions are on (right panel) compared with the control case (all emissions) (left panel).

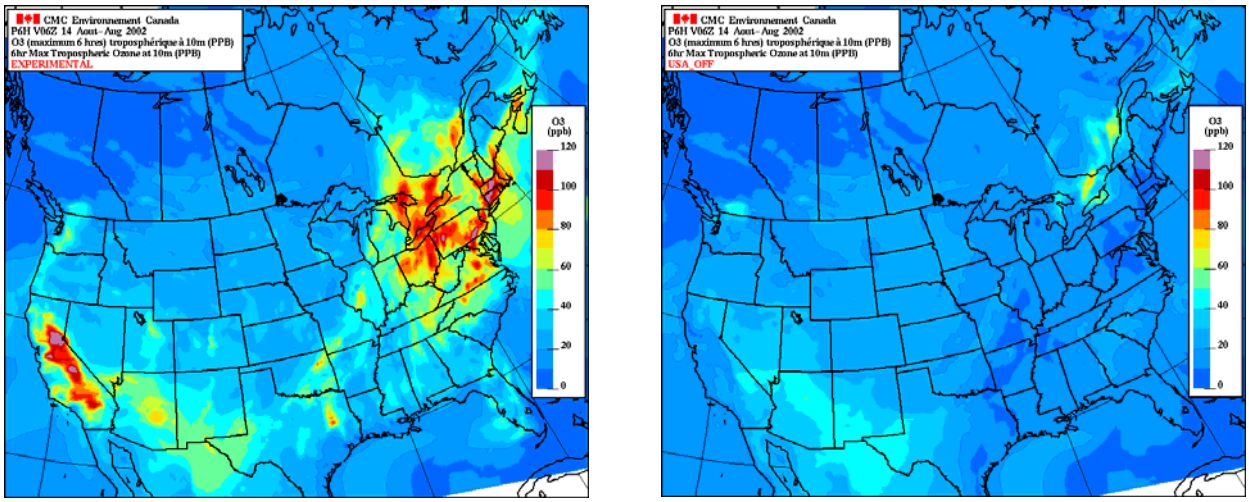

Figure 3 Emissions scenario. Left panel control case, all emissions on. Right panel, only Canadian emissions are on.

4. Optimum interpolation of surface ozone measurements

The development of ozone analyses is little motivated to improve forecast, since ozone is an end product in chemical reactions, changes in the initial condition has a rather small impact of the prediction. The real motivation rather arises from other reasons: 1- because of the large amount of ozone in the stratosphere, the tropospheric ozone information derived from satellite observations is generally weak, noisy and requires additional assumptions to be retrieved. The situation is worse with ozone in the surface layer, and thus surface ozone measurements provide useful and complementary information to satellite observations. 2 – the surface ozone measurement are also very accurate with very little bias (<1 ppb), the instruments are robust and calibrated each night at many sites. The observation network is fixed in space, and reports are available

each hour. These characteristics make the surface ozone observations network ideal for the construction of error covariances that is needed for data assimilation. 3 – The ease of implementation of the optimum interpolation scheme and small size of the estimation problem (~ 1500 observations /hour) is a distinct advantage to quickly develop a scheme for operational production.

The comparison with observations, which is necessary in the development an assimilation system, is an important diagnostic to improve the quality of the model. During the last few years, several changes were made to the model. At the beginning of the exercise, the average bias was about 10-15 ppb and this was almost the same size as the standard deviation. And this situation is in contradiction with the usual assumption of data assimilation that model and observations should be unbiased, or that the bias is small compared with the standard deviation. This situation needed to be corrected before any implementation of the assimilation system could take place. Currently, the average bias is about 3-5 ppb (after we performed a bias correction) and roughly about an order of magnitude smaller than the standard deviation.

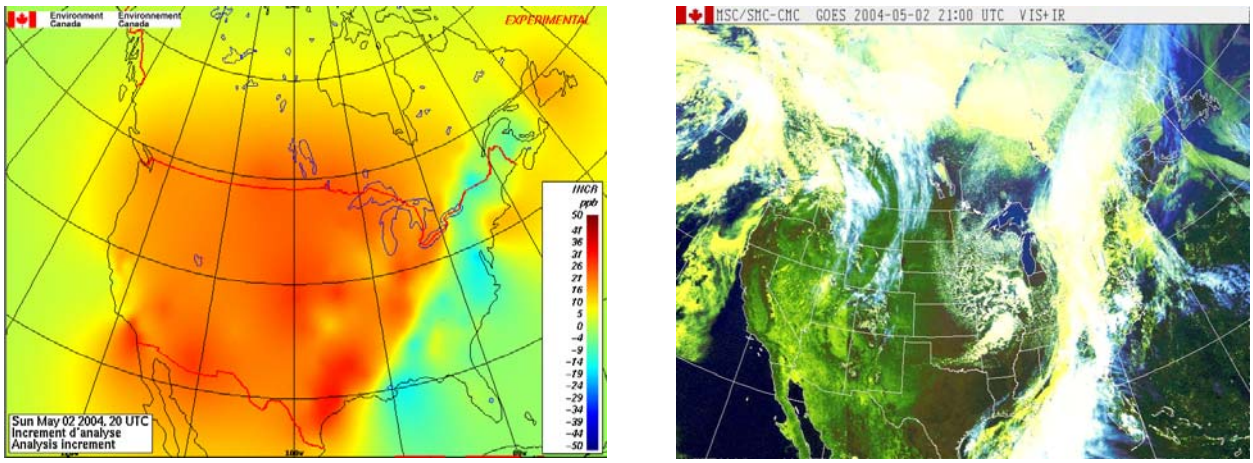

Figure 4 Case study May 2, 2004. Analysis increment at 20 UTC (left panel). Cloud visible channel for GEOS at 21 UTC (right panel)

Spatially organized or temporal persistent analysis increments are generally an indication of a systematic model or observation error. The left panel of figure 4 shows the analysis increment on a particular date and time. We observe a large negative analysis increment over eastern North America, and correspondingly a thick cloud deck over the same area (right panel). Because of the low top of the model (6 km), higher clouds above the top were not accounted in the CTM and this effect might explain the negative increment analysis associated with the frontal cloud structure.

4.1. Implementation of the optimum interpolation scheme

Optimum interpolation (OI) is an approximation to the steady-state Kalman filter. The scheme was developed by Gandin (1963) and applied to operational meteorological forecast by Rutherford (1972). The scheme is described in Ménard (2000) along with a discussion on issues about covariance modelling. The equations consist in a short-term forecast of the state,

$$\mathbf{x}_{n+1}^{f} = \mathbf{M}_n \mathbf{x}_n^{a} \tag{1}$$

followed by an analysis,

$$\mathbf{x}_n^{a} = \mathbf{x}_n^{f} + \mathbf{K}_n(\mathbf{y}_n - \mathbf{H}_n \mathbf{x}_n^{f}) \tag{2}$$

$$\mathbf{K}_n = \left\{ \vec{K}_n(i) \right\} \tag{3}$$

$$\vec{K}_n(i) = \vec{B}(r_i, \mathbf{r}_{obs})\left[\mathbf{B}(\mathbf{r}_{obs}, \mathbf{r}_{obs}) + \mathbf{R}\right]^{-1} \tag{4}$$

where i = 1, …, N (number of model grid points), $\vec{K}$ is a row vector of dimension p (number of observations) of Kalman gain, r_i is the position of the grid point i, $\mathbf{r}_{obs}$ is a vector of position of the observations, **y** is the observed values, **x** is the model state, and superscripts a and f designate the analysis and forecast respectively.

The information about observation and background error statistics is obtained from innovations, i.e. differences between observations and model values — this will be explained in detail the next paragraph. In an optimum interpolation scheme, the observation operator applied on the background error covariance is never actually calculated explicitly. Rather, for point observations, the application of the observation operator on the error covariance amounts to evaluate directly the error covariance at the observation locations. Using innovations, it is then possible to derive most of the error statistics needed in the evaluation of (4), except for $\vec{B}(r_i, \mathbf{r}_{obs})$. This last quantity represents the covariance of the background error between model grid points and observation locations. This quantity can only be obtained from modelling. Usually a correlation function is a fitting at the observation location, and the background error variance is interpolated (or smoothed) from the background error variance evaluated at the observation locations. These are the main characteristics of an optimum interpolation scheme. On the other hand, when the number of observations is large (e.g. exceeds about 1500) the matrix inversion in (4) cannot be obtained numerically. Data selection is then used to reduce the number of observations in the covariance matrix.

Under certain assumptions, it is possible to obtain the background and observation error statistics from the innovations. Indeed, the observed value can be thought of as the true value plus an observation error, and likewise, the model value (or background value) can be though of the true value plus the model (or background) error. The innovation that is the observation minus the model value is then equal to the observation error minus the background error. By constructing spatial covariance of innovations it is usually possible to distinguish the observation error part form the background error part as follows. For each observation location and within a circle of influence of typically 1000 km, (see figure 5) we compute the innovation covariance as a function of distance.

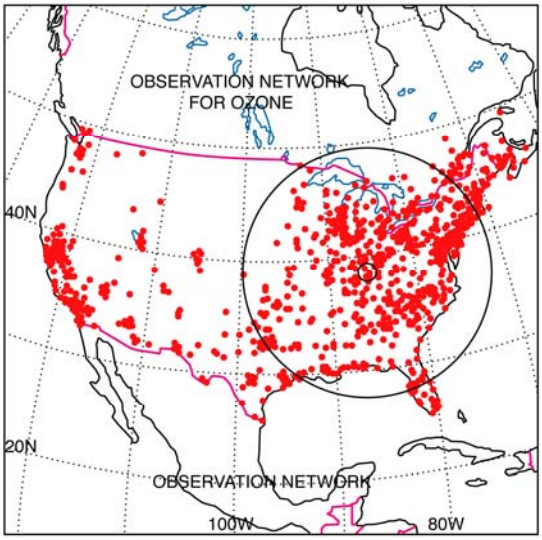

Figure 5 Area of selection to construct the spatial error covariance of innovations. Data over a month is used to compute these statistics using all observations within a radius increment (in figure 6, variances were averaged over a 30 km bin).

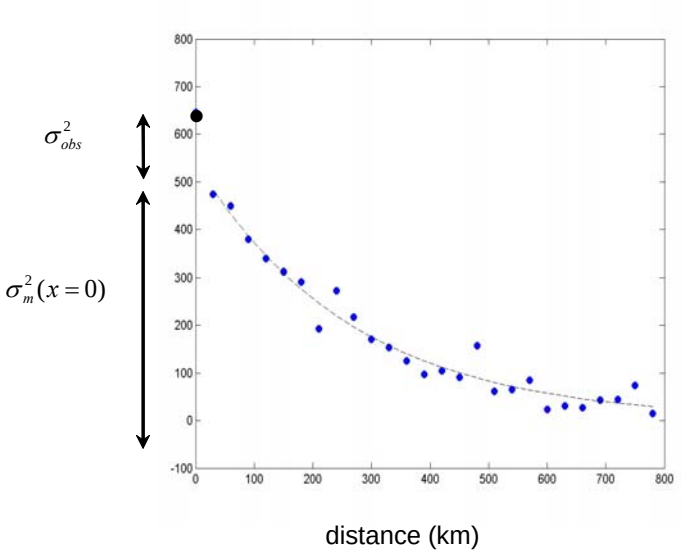

Figure 6 Innovation covariance as a function of distance.

We observe that the covariance roughly follows a decorrelation curve as a function of distance except at the origin, where there is a jump in the covariance value. This jump is an indication that the innovation is a combination of a spatially correlated and spatially uncorrelated contribution. The latter is assumed to be due to the observation error and the background error is assumed to be spatially correlated. Standard correlation models such as autoregressive model (see Daley 1991) are fitted to the spatially correlated portion of the data. The intercept then represents the model error variance at the observation location, and the difference between the innovation variance (at the origin) and the intercept is the observation error variance. One way to perform the fitting is to minimize the following cost function

$$\begin{aligned} J(L(i),\sigma_B(i)) &= \sum_{j\neq i}\Big(\langle OmF_i\rangle\langle OmF_j\rangle - \sigma_B(i)\sigma_B(j)\ C(i,j)\Big) \\ &\approx \sum_{j\neq i}\Big(\langle OmF_i\rangle\langle OmF_j\rangle - \sigma_B^2(i)\ C(i,j)\Big) \end{aligned} \tag{5}$$

with respect to *L(i)*, the correlation length scale of a given correlation model, and $\sigma_B(i)$ the model error standard deviation at the observation location i . In the last expression we have made the assumption that the error variance varies smoothly in space such that in the minimization we can replace $\sigma_B(j)$ by $\sigma_B(i)$, which allows the fitting procedure to be done at each observation location independently of the others. An example of the cost function (5) is given in figure 7.

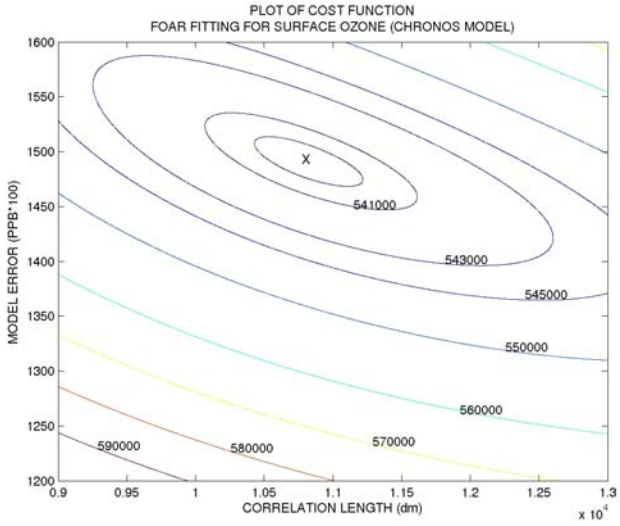

Figure 7 Cost function (eq. 5) at a station, as a function of L and σ_B

Several correlation models were used in the fitting, and we found out that the first order autoregressive model (FOAR) achieved the best result. The FOAR is of the form

$$C(i,j) = \exp\left(-\frac{|r_i - r_j|}{L}\right) \tag{6}$$

It is important to note that error variances and correlation model are needed in order to conduct an assimilation experiment, but the innovations that are needed to conduct the fitting can only be derived from an assimilation experiment. To solve this problem an iterative procedure is applied until convergence between the assumed error statistics that made up the Kalman gain (i.e. input of the assimilation system) are in agreement with the innovations (i.e. output of the assimilation system). First we begin with **Pass 0** where the difference between observation and model value is done without any assimilation system in place. With this information, error variances and correlation are obtained, Kalman gain can then be computed, and an assimilation run can then be executed. In **Pass 1**, the innovations of the assimilation in **Pass 0** are used to derive new error statistics. We reconduct the assimilation in **Pass 2** using innovation of **Pass 1** to construct the error variances and correlation. The procedure usually converges adequately at **Pass 2**. That is when

$$\left\langle OmF_i, OmF_j \right\rangle \approx B(r_i, r_j) \quad \text{for } i \neq j \tag{7}$$

To compute the Kalman gain, further assumptions need to be made in order to obtain:

1. the model error covariance between the model grid points and the observation locations $\vec{B}(r_i, \mathbf{r}_{obs})$. The simplest solution is to use a uniform error standard deviation for the error standard deviation at the grid points, i.e. for a given pair of points *i* for a model grid point, and *j* for an observation location

$$B(r_i, r_j) = \sigma_B(r_i)\, \sigma_B(r_j)\, C(r_i, r_j) \approx \bar{\sigma}_B\, \sigma_B(r_j) C(r_i, r_j) \tag{8}$$

2. a positive definite correlation model. The simplest solution is to use a homogeneous model. We use the average correlation length scale obtained from the fitting procedure,

$$L = \bar{L}(r_j) \tag{9}$$

4.2. Statistical consistency

A way to verify the statistical consistency is to look at the residuals $\left\langle (OmF)^2 \right\rangle - (diag(\mathbf{B}) + \mathbf{R})$ normalized by innovation variances to assess how consistent the input statistics is with the output statistics. Another measure is χ^2 (Ménard and Chang, 2000). In a statistically optimal system, the expected value of χ^2 should be equal to the number of observation p, i.e.

$$\left\langle \chi^2 \right\rangle = \left\langle \mathbf{d}^T (\mathbf{B}+\mathbf{R})^{-1} \mathbf{d} \right\rangle = p \tag{10}$$

A single analysis gives only one realization of χ^2. However, the statistical variation is this random variable depends directly on the sample size, that is *p*, and for most practical purposes this is quite small, so that χ^2 compute for each analysis should remain close to p. Figure 8 below, shows the time evolution of for a period of about one month. The gray zone represents the error bar that can be attributed to the statistical fluctuation of the quantity (based on the sample size).

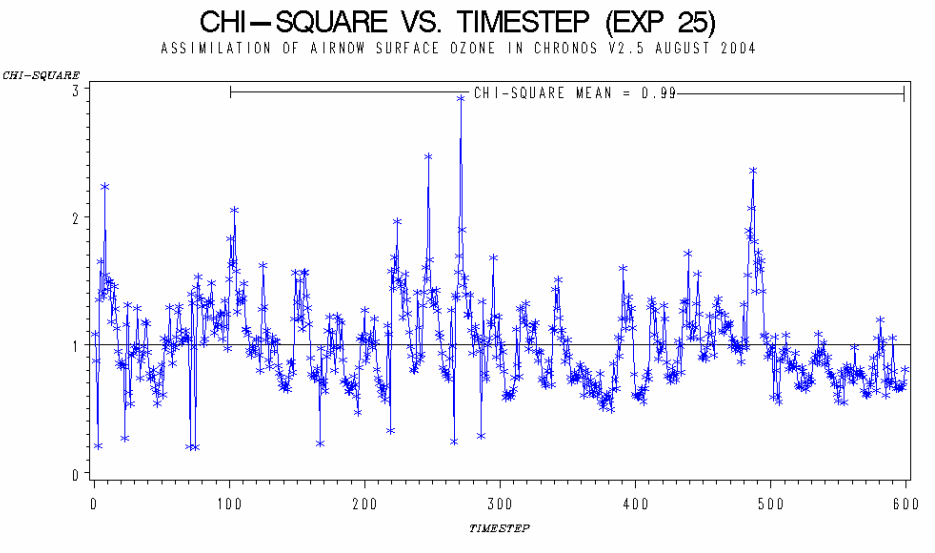

Figure 8 Time evolution of χ^2 / p

The power spectrum of χ^2 / p is also a useful diagnostic tool, as it reveals deficiency in the assimilation system. For instance, we observe a 24 h power peak in χ^2 / p, which correspond with the refresh rate of the meteorological analyses used to drive the CTM.

4.3. Verification

To validate the analyses, we conduct the assimilation with a subset of the observations and use the remaining observations to compare with the analyses. However, the error statistics needs to be reconducted when a subset of the observation is used, since the observations and their number have an influence on how much error reduction can be achieved in an assimilation.

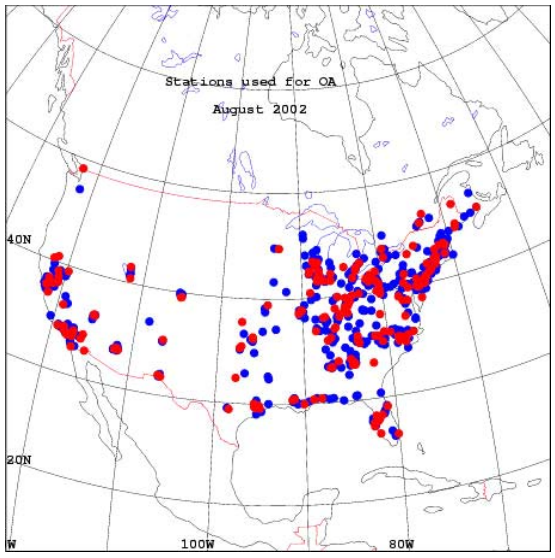

Figure 9 Red dots are the observations used for the validation. Blue dots are observations used to produce the analyses.

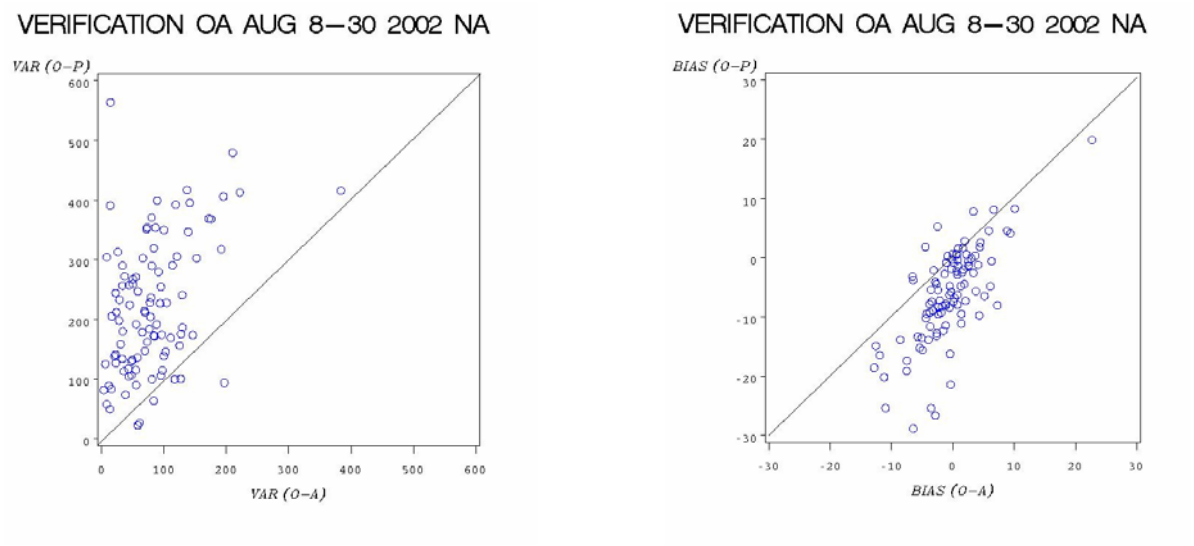

Figure 10 Verification of the ozone objective analysis. Left panel is the standard deviation before (O-P) and after the analysis (O-A). Right panel is the bias before (O-P) and after analysis (O-A).

Figure 9 shows the spatial distribution of the observation used for verification (red dots) (1/3 of the observations), and in blue the observations that were used to perform the analyses (2/3 of the observations). In figure 10 is depicted the error statistics (O-P) before and after the analyses (O-A). On the left panel, we observe that most of the verification points are above the diagonal line indicating a reduction of error variance of observed minus model residuals as a result of the analysis. As an average, the reduction of variance is of the order of a factor of 2. For few stations, the reduction of variance is over 5 times. On the right panel, the range of the bias before analysis (ordinate) is larger than the range of values after the analysis (abscissa).

4.4. Background vertical error correlation

The innovations themselves give very little information about the vertical correlation of the background error, since all the observations are at the surface. However, information about the vertical correlation length scale can be obtained by minimizing the forecast error in assimilation runs. Figure 11 below, shows the average O-P and O-A over a three week assimilation period for different vertical correlation length. A weak minimum is obtained for a correlation length scale of about 1 km which corresponds to an average height just above the height of the boundary layer

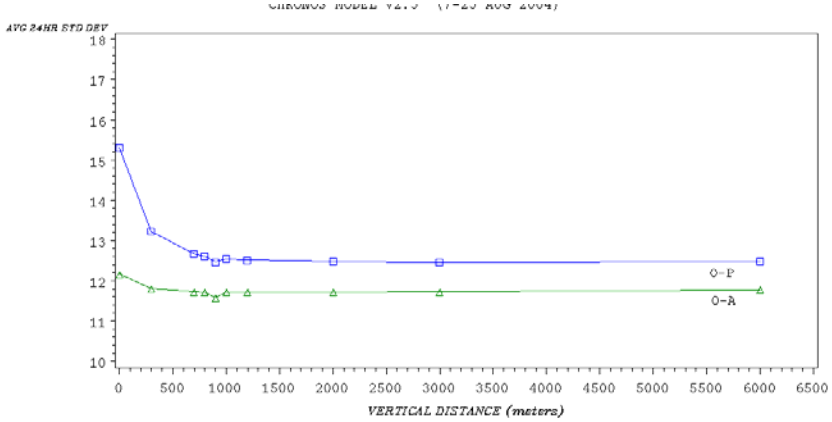

Figure 11 Impact of changing the vertical correlation length scale

5. Prediction

An obvious application of data assimilation is to examine its the impact of the prediction. Experiments were conducted where the assimilation were conducted from 00Z to 06Z, from 00Z to 12Z, and continuously (00Z-23Z).

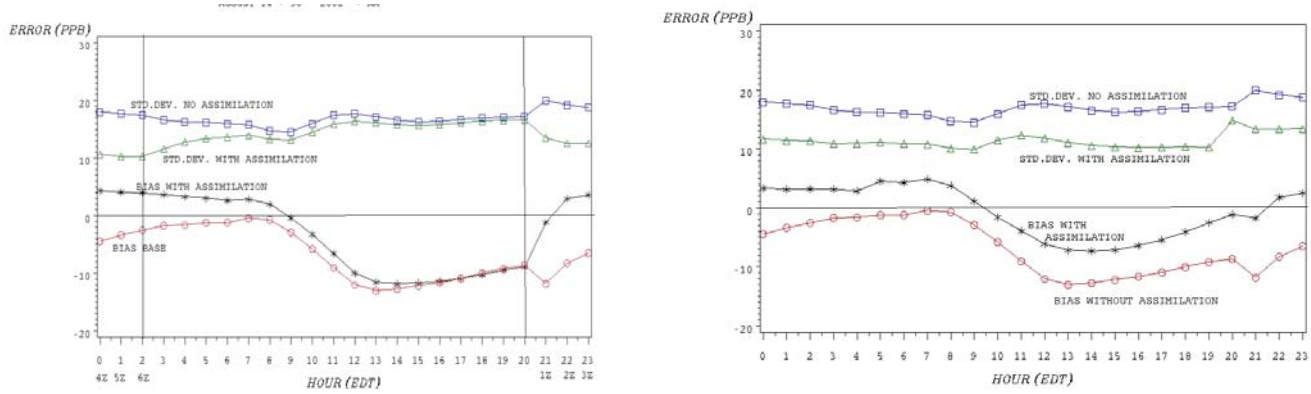

Figure 12 Impact of ozone analysis on prediction. Left panel assimilation from 00Z to 06Z. Right panel continuous (24h) assimilation.

These results corroborate the finding of others that the impact of ozone observations in a simple univariate scheme (as the one implemented here) is limited in time. An examination of the impact of ozone assimilation on precursors species (e.g. NO, NO2) and also on related species (OH and O) turn out to be very small. As a result and since ozone prediction is driven to a large extent by its precursors, thus even if initially the ozone concentrations are changed as a result of the analysis after a period of about six hours the ozone becomes controlled by its precursors and then shown little to no impact on the analysis.

6. Environmental impact

An important environmental impact of ozone is its deposition on vegetation, which influences growth and health. In particular, the surface flux of ozone is the key parameter.

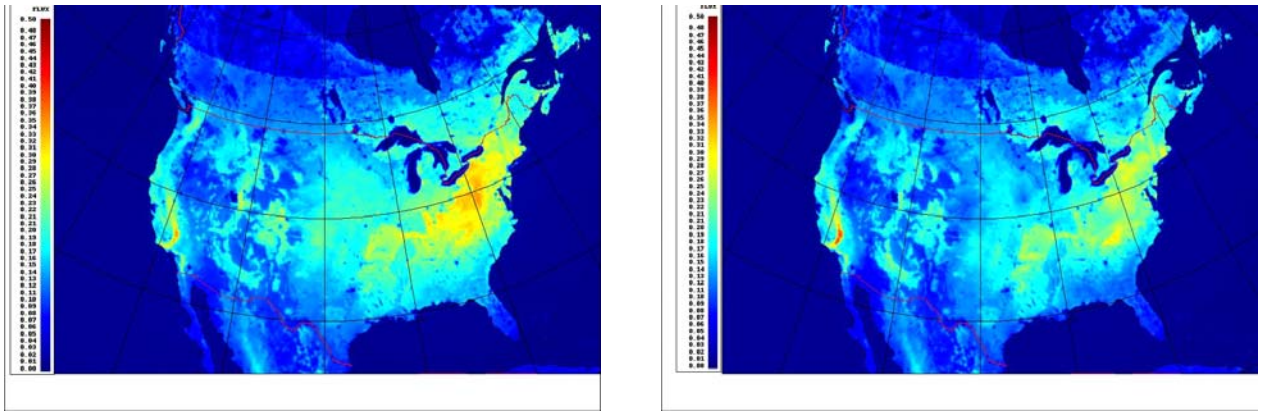

Figure 13 Average flux of ozone at the surface for the period 7-30 August 2002. Left panel no assimilation. Right panel with assimilation of ozone.

In the above figure, we depict the surface flux of ozone with the model with no assimilation and with assimilation of ozone.

7. Assimilation vs Monitoring: How important is chemical modelling ?

In a series of experiments we have assessed the importance of chemical modelling in assimilation of ozone. The statistics presented below were obtained by comparing the analyses (or one hour forecast) with the data that was not assimilated (as in section 4.3). First lets examine the results when we assimilate with chemistry.

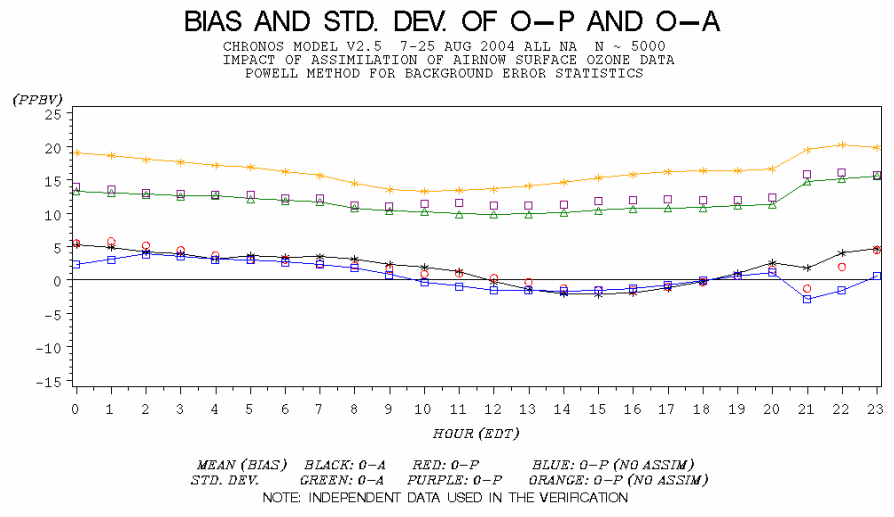

Figure 14 Verification statistics with chemistry in the CTM – control run.

In figure 14, the upper curves are standard deviation and the curves around the zero line are biases. The yellow and blue curves represent the standard deviation and bias respectively for the free model run (i.e. no assimilation). With assimilation the O-P standard deviation (purple squares) is reduced from 20 ppb to about 15 ppb, whereas the bias remains unchanged. The standard deviation O-A (green line) is also a bit smaller than the O-P standard deviation. The O-A bias is about the same as O-P and free model run biases.

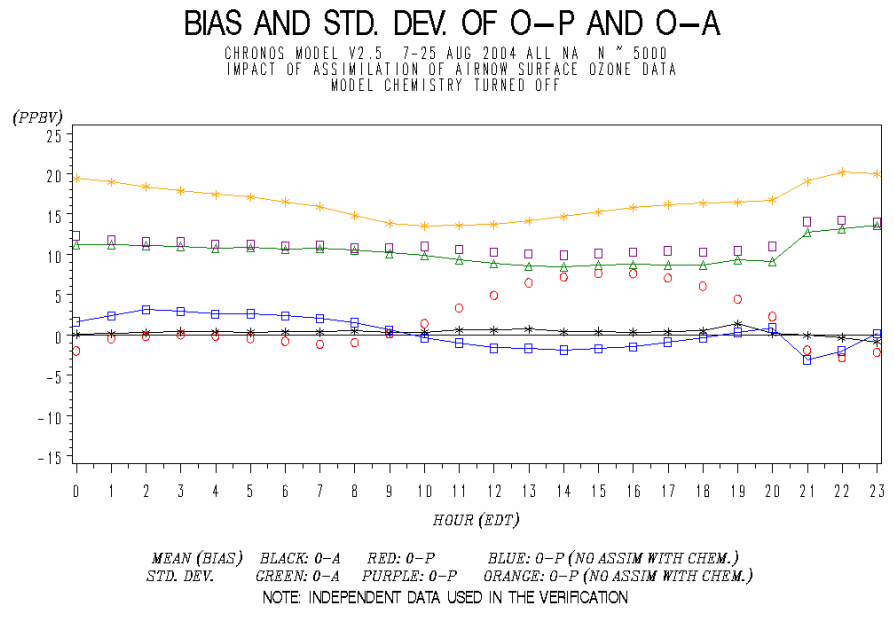

Figure 15 Verification statistics with no chemistry in the CTM.

In figure 15, a similar diagnostic was produced for an assimilation with the same CTM but with the chemistry turned off. The free model run with chemistry is also reproduced in figure 15 (same as in figure 14) with the yellow and blue curves. The black line and green line represents the O-A bias and standard deviation respectively. We note that the error standard deviation has been reduced from 20 ppb (no

assimilation) to about 12 ppb (in assimilation with no chemistry). The standard deviation reduction is actually greater when there is no chemistry then with chemistry. The O-A actually represents the quality of monitoring. In this context, we are looking at the ability of the system to infer ozone at locations away from observations. The O-P on the other hand, look at the error statistics associated with the model prediction (and also away from the observations).

The bias is depicted with red circles and the standard deviation with the purple squares. We note that during daytime, a very large bias develops, and that is with only one hour prediction. In summary, for monitoring purposes, the verification statistics derived from O-A reveals the without chemistry the reduction of error variance is greater and the bias is smaller, than if chemistry was used in the CTM. For forecasting however, large daytime bias develops in a matter of only one hour of prediction.

8. Ongoing and future direction

In these experiments we have explored the possibilities offered by data assimilation. It has become quite apparent that in order to continue to improve chemical forecast, we need to remove some of the limitations of limited area and offline modelling. Over the last year the Meteorological Service of Canada has been developing an online chemistry with the operational weather prediction model GEM (Global Environmental Multiscale model) and extend the 3D Var analysis system to include chemical species, and have adapted the observation data format and tools used in operations to chemical species. Ongoing work deals with stratospheric chemical data assimilation where in particular we examine the effect of cross error covariance between chemistry and dynamics, in the assimilation of Envisat data. Our next phase of development will address more specifically the troposphere, were 4D Var capability will be developed to control chemical concentrations but also surface fluxes.

9. References

Daley R., 1991: Atmospheric Data Analysis. Cambridge University Press. 457 pp.

Gal-Chen T. and Sommerville, R.C., 1975. On the use of a coordinate transformation fro the solution of Navier-Stokes equations. J. Comp. Phys., 17, 209-228.

Gandin, L, 1963: Objective Analysis of Meteorological Fields (Leningrad: Gridromet). English translation (Jerusalem: Israel Program for Scientific Translation), 1965.

Lurmann, F.W., Lloyd A. C. and Atkinson R., 1986. A chemical mechanism for use in long-range transport/acid deposition computer modelling. J. Geophys. Res. 91, 10905-10936.

Ménard, R., 2000: Tracer assimilation. In Inverse Methods in Global Biogeochemical Cycles, eds. Kasibhatla et al.. AGU Press, p 67-80.

Pudykiewicz, J., Kallaur A., Smolarkiewicz K., 1997. Semi-Lagrangian modeling of tropospheric ozone. Tellus, 49B, 231-248.

Rutherford, I, 1972: Data assimilation by statistical interpolation of forecast fields. J. Atmos. Sci., 29, 809-815.